Full Length Article

Poisoning effects of H₂S and HCl on the naphthalene steam reforming and water-gas shift activities of Ni and Fe catalysts

Xiaomin Dou[a], Andrei Veksha[a,*], Wei Ping Chan[a], Wen-Da Oh[a,b], Yen Nan Liang[c], Florence Teoh[a,d], Dara Khairunnisa Binte Mohamed[a,e,f], Apostolos Giannis[a,g], Grzegorz Lisak[a,e], Teik-Thye Lim[a,e,*]

[a] Residues and Resource Reclamation Centre, Nanyang Environment and Water Research Institute, Nanyang Technological University, 1 Cleantech Loop, Clean Tech One, Singapore 637141, Singapore
[b] School of Chemical Sciences, Universiti Sains Malaysia, 11800 Penang, Malaysia
[c] Environmental Chemistry and Materials Centre, Nanyang Environment and Water Research Institute, Nanyang Technological University, 1 Cleantech Loop, Clean Tech One, Singapore 637141, Singapore
[d] School of Chemical & Life Science, Nanyang Polytechnic, 180 Ang Mo Kio Avenue 8, Singapore 569830, Singapore
[e] School of Civil and Environmental Engineering, Nanyang Technological University, 50 Nanyang Avenue, Singapore 639798, Singapore
[f] Interdisciplinary Graduate School, Nanyang Technological University, 50 Nanyang Avenue, Singapore 639798, Singapore
[g] School of Environmental Engineering, Technical University of Crete (TUC), Politechnioupolis, 73100 Chania, Greece

ARTICLE INFO

ABSTRACT

H₂S and HCl are common impurities in raw syngas produced during gasification of biomass and municipal solid waste. The purpose of this study was to investigate the poisoning effect of H₂S and HCl on synthesized and commercial catalysts during steam reforming of naphthalene. Four synthesized catalysts with different loadings of Ni and Fe on alumina support and two commercial catalysts were selected and evaluated in a fixed bed reactor at 790, 850 and 900 °C. The obtained results revealed that reforming and water-gas shift (WGS) activities of catalysts did not benefit from the Fe addition. The activities were influenced differently by H₂S and HCl indicating that the reactions were catalyzed by different active sites on the nickel surface. In the presence of H₂S and HCl, the poisoning of naphthalene reforming activity was caused by H₂S and was not affected by HCl when both compounds were present in the gas. H₂S chemisorbs on nickel surface forming NiS and decreasing the accessibility of active sites to hydrocarbons. The poisoning effect was only partially reversible. On the contrary, the poisoning of WGS activity could be caused by both H₂S and HCl, and the activity could be completely restored when H₂S and HCl were removed from the gas. Unlike naphthalene reforming activity, which was comparable for catalysts with similar Ni loadings, WGS activity depended on the catalyst structure and was less susceptible to poisoning by H₂S and HCl in case of the catalyst with strong NiO-support interactions.

1. Introduction

Syngas obtained during biomass/municipal solid waste (MSW) gasification is mainly a mixture of carbon monoxide, carbon dioxide, hydrogen, methane and nitrogen, which can be utilized for electric power generation or liquid fuel synthesis [1]. The biomass- and MSW-derived syngas, however, contains significant concentrations of impurities such as tar, HCl, alkali chlorides, particulate matter, ammonia, HCN and sulfur compounds. Tar, consisting of a mixture of aromatic hydrocarbons, causes equipment failure by its condensation and corrosion upon cooling of syngas [2–4]. The techniques that can efficiently remove tar compounds to the acceptable levels are still under development. One of the prospective techniques is catalytic steam reforming which converts tar into H₂ and CO [5–7]. Different types of natural minerals (e.g., dolomite, olivine and clay minerals) and synthetic catalysts (e.g., char, activated alumina and metal-based catalysts) were proposed for tar reforming, among which Ni-based catalysts are the most common and commercially available. The utilization of Ni-based catalysts enhances syngas production due to steam reforming of hydrocarbons and other catalyzed reactions, including dry reforming, WGS and Bodouard reactions [8–12]. Furthermore, Ni-based catalysts facilitate simultaneous decomposition of NH₃ and HCN into N₂ and H₂

during the reforming process, resulting in lower NOx emissions [13,14].

Besides nickel, other metals as well as bimetallic and polymetallic composites have been extensively investigated as reforming catalysts [15–23]. For instance, monometallic Fe and bimetallic Ni-Fe catalysts have shown satisfactory reforming activity and high catalytic stability during reforming of tar compounds under certain conditions [24–28]. Noichi *et al.* [24] found that higher Fe content in Fe-Al catalysts enhanced the catalytic steam reforming activity by increasing naphthalene conversion efficiency. In NiO–Fe$_2$O$_3$–Al$_2$O$_3$ catalysts developed by Dong *et al.* [25] and Margossian *et al.* [26], syngas production and dry reforming activities of methane were influenced by Fe content. Furthermore, catalysts with optimized Fe content were reported to enhance thermal stability of the Ni-Fe catalysts by mitigating coke formation during tar reforming [25,26]. This superior effect was attributed to the formation of Ni-Fe alloys enriched with Fe-O species at the surface of nanoparticles that could catalyze coke oxidation [27,28].

It is well known that impurities present in syngas (e.g., particles, sulfur and chlorine species) can poison the catalysts during steam reforming process [29–35]. H$_2$S is notorious poison for catalysts and only a few ppmv of H$_2$S could rapidly deactivate a Ni-based reforming catalyst [29–32]. Upon contact with Ni-based catalyst, sulfur species (e.g., H$_2$S) chemisorb on metal sites forming NiS according to the reaction (1) decreasing the accessibility of active sites to hydrocarbons [29]:

$$Ni + H_2 S \rightleftharpoons Ni - S + H_2 \qquad (1)$$

Yung *et al.* [30] have attempted to regenerate the spent Ni catalyst which was contaminated during catalytic tar reforming at 850 °C by 43 ppmv H$_2$S in syngas produced from gasification of white oak. It was found that the Ni-S species in catalyst could not be completely removed during the steam/air regeneration procedure. As a result, the catalytic activity of Ni was only partially recovered and was lower than its initial activity levels [30]. The low melting point and high surface mobility of NiS can accelerate sintering [31], which may deteriorate the activity of catalyst. Furthermore, sulfur species can increase the carbon deposition on catalyst surface, which also decreases the catalytic activity [32].

The presence of HCl in syngas was reported to decrease the reforming and WGS activities of Ni catalysts [33–37]. Richardson *et al.* [33] found that the conversion of methane was extremely inhibited in the presence of HCl, due to the chemisorption of HCl by Ni. Coute *et al.* [36] demonstrated that HCl induced detrimental effect on WGS activity during steam reforming of chlorocarbons. Veksha *et al.* [37] investigated the mechanism for the activity loss of Ni catalysts during naphthalene reforming in the presence of 2000 ppmv HCl and demonstrated that naphthalene conversion is not influenced by HCl while WGS activity was poisoned due to the sintering of Ni. In the above mentioned studies, either H$_2$S or HCl were present in gas streams during the reforming while in real syngas, these impurities are present simultaneously. To what extent the co-existence of both H$_2$S and HCl in the gas can influence the catalytic activity during steam reforming has not yet been investigated.

The purpose of this work was to investigate the influence of H$_2$S and HCl on the poisoning of synthesized and commercial catalysts during steam reforming of tar. It has been well known that Ni is an excellent metal for steam tar reforming. In this study, the addition of Fe is attempted, because Fe is a low cost material and Fe species has high redox activity [38]. Furthermore, the addition of Fe to Ni had beneficial effect on the performance of bimetallic catalysts under certain experimental conditions [24–28]. Four synthesized catalysts with different loadings of Ni and Fe on alumina support and two commercial catalysts were tested in a fixed bed reactor at different temperatures with varying contents of H$_2$S and HCl in gas. Naphthalene was used as a model tar compound as it is one of the major tar species [39] which also has high stability during tar reforming [40–42]. In this study, 50 ppmv H$_2$S and 300 ppmv HCl were used as they are in the range of typical concentrations of H$_2$S and HCl present in syngas produced from biomass/MSW [29–31,34–37]. The individual and combined effects of impurities on reforming and WGS activities of the catalysts and the reversibility of the catalyst poisoning are discussed.

2. Materials and methods

2.1. Catalysts

Four catalysts with different Ni and Fe contents were synthesized using the method described elsewhere [37]. Briefly, the catalysts were prepared by impregnation of aluminum hydroxide (H$_3$AlO$_3$·xH$_2$O, Sigma-Aldrich) having particle sizes of 0.56–1.18 mm with known concentrations of Ni(NO$_3$)$_2$·6H$_2$O (Sigma-Aldrich) and Fe(NO$_3$)$_3$·9H$_2$O (Sigma-Aldrich) in aqueous solution. After evaporation of water in a rotary evaporator (Hei-Vap Precision, Heidolph Instruments, Germany), the materials were dried overnight in an oven at 105 °C and calcined at 500 °C for 2 h (heating rate 2 °C min^{-1}) in air, followed by sieving to obtain particle sizes between 0.56 and 1.18 mm. The synthesized catalysts are denoted as xNi − yFe, where x and y represent calculated molar contents of metals per 100 g of the resulted catalyst.

Two commercial catalysts from different manufacturers (6-holes monoliths from Xian Sunward Aeromat Co., China and 19 × 19 × 10 mm rings from Pingxiang Hualian Chemical Ceramic Co., China) were crushed and sieved to obtain 0.56–1.18 mm particles, and used as the reference materials.

2.2. Naphthalene reforming

Fig. 1 shows the experimental setup for catalytic naphthalene reforming. A fixed bed reactor with a quartz frit (50–90 μm openings) was used. In a typical run, 0.5 mL of a catalyst was loaded into the reactor and heated at 15 °C min^{-1} in reducing atmosphere containing 20 vol% H$_2$ – 80 vol% N$_2$ (total gas flow 50 mL-STP min^{-1}) to the reforming
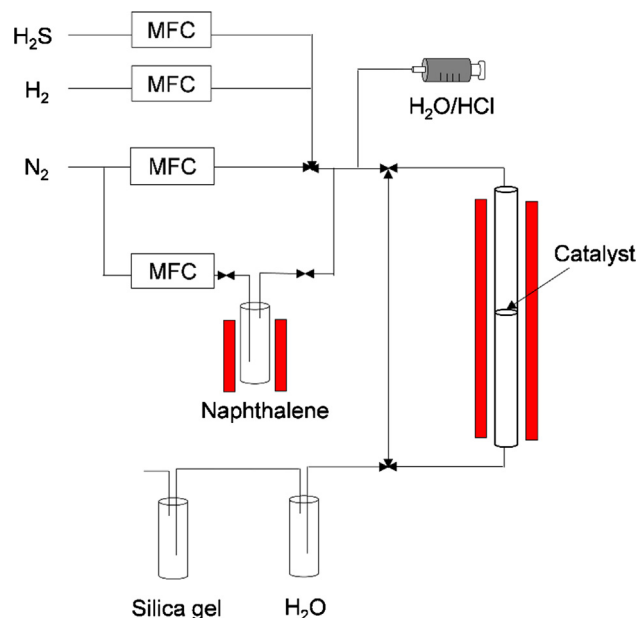

Fig. 1. Bench-scale catalytic steam reforming setup.

temperature of 790, 850 or 900 °C. Once the temperature was reached, the gas flow was maintained for 30 min to reduce the catalyst and then the flow was switched to 200 mL-STP min^{-1} (space velocity 24,000 h^{-1}) of a model syngas containing 0.14 vol% naphthalene, 10 vol% H_2, 26 vol% H_2O, 0 or 300 ppmv HCl, 0 or 50 ppmv H_2S and N_2 (balance). In this study, 0.14 vol% naphthalene was used as it is within the range of typical concentrations of naphthalene produced from biomass/MSW gasification [43,44]. Naphthalene vapors were generated by purging N_2 gas through an evaporator containing heated naphthalene. H_2, N_2 and H_2S were supplied from gas cylinders using mass flow controllers. The steam and HCl vapor were generated from aqueous solution of HCl injected by a syringe pump into an evaporator. During experiment, all the gas lines were heated and kept above 150 °C to avoid vapor condensation. After reforming reactor, the model gas passed through two water traps to capture HCl and one silica gel trap to remove moisture, and then was collected in Tedlar gas bags for analysis (collection time 5 min). Concentrations of CO, CO_2 and C_1-C_5 hydrocarbons were measured by a calibrated gas chromatograph (Agilent 7890B, USA) equipped with one flame ionization and two thermal conductivity detectors. Steam reforming of naphthalene is analogous to steam reforming of other hydrocarbons [10,45]:

$$C_{10}H_8 + 10H_2O = 10CO + 14H_2 \tag{2}$$

Due to WGS activity, CO is partially converted to CO_2 over Ni catalysts [1,28,45]:

$$CO + H_2O = CO_2 + H_2 \tag{3}$$

Naphthalene conversion can be calculated by the following equation:

$$\text{Naphthalene conversion } (\%) = \frac{(n_{CO_2} + n_{CO})}{n_{naphthalene} \times 10} \times 100\% \tag{4}$$

where: n_{CO} and n_{CO_2} are the molar concentrations of CO and CO_2 generated during steam reforming of naphthalene, mol min^{-1}, and $n_{naphthalene}$ is the molar concentration of naphthalene in the feed, mol min^{-1}. All experiments were triplicated and the results are presented as averages of three experimental runs.

2.3. Characterization of catalysts

The catalysts were characterized by X-ray diffraction analysis with Cu-Kα radiation source (XRD, Bruker AXS D8 Advance), X-ray photoelectron spectroscopy with a dual anode monochromatic Kα excitation source (XPS, Kratos Axis Supra), X-ray fluorescence spectroscopy (XRF, PANalytical Axios mAx), transmission electron microscopy at 120 kV (TEM, JEOL JEM-2010) and N_2 adsorption at −196 °C (Quantachrome Autosorb-1 Analyzer). Binding energies of elements in XPS spectra were corrected against an adventitious carbon C 1s core level at 284.8 eV. The processing of XPS peaks was carried out in the CASA XPS software. TEM images were used to measure the size of Ni nanoparticles in spent catalysts. The diameters were calculated using ImageJ software by analysing 150–200 Ni nanoparticles in each sample and assuming that

nanoparticles have ideal spherical shape. Specific surface area of catalysts was calculated from N_2 adsorption isotherms using BET model. Total pore volumes were calculated from N_2 adsorption volume at P/P_0 = 0.96. Temperature programmed reduction (TPR) was performed in a 5% H_2/N_2 gas mixture at 30 mL min^{-1} flow rate with a temperature ramp of 10 °C min^{-1} up to 900 °C. Carbon content in the catalysts was measured by CHNS elemental analyser (Vario EL Cube).

3. Results and discussion

3.1. Properties of catalysts

The properties of pristine Ni, Fe, Ni-Fe and commercial catalysts are presented in Table 1. Ni and Fe contents were determined from XRF analysis and used to calculate molar quantities of Fe and Ni. The molar Ni and Fe loadings per 100 g of catalysts were close to the corresponding theoretical values of x and y in xNi-yFe samples. The amount of Ni in 0Fe-0.4Ni and two commercial catalysts loaded into the reactor for steam reforming of naphthalene was nearly the same (approx. 1.90 mmol 0.5 mL^{-1} catalyst) due to the differences in bulk density, allowing comparison between the activities of Ni in the synthesized and commercial catalysts. The synthesized catalysts had higher BET specific surface areas and total pore volumes compared to the commercial catalysts. According to the high N_2 adsorption volumes at relative pressures P/P_0 > 0.1 and hysteresis loops between adsorption and desorption branches of isotherms (Fig. S1), the synthesized materials were mesoporous. Among them, 0Fe-0.4Ni had the largest porosity (i.e. 213 m^2 g^{-1} and 0.31 mL g^{-1}, respectively) (Table 1), which is one of the reasons for its better catalytic performance stated in the following study. The specific surface areas and total pore volumes of the synthesized catalysts decreased with increasing Ni + Fe contents, which can be attributed to the impregnation of the porous alumina with loaded metal species. X-ray diffraction (XRD) patterns of the synthesized catalysts in Fig. 2 consist of broad peaks with no distinct XRD peaks and also show no sharp XRD peaks indicating that alumina, nickel and iron oxides have non-crystalline and/or nanosized structures, so that alumina provides surface area for better dispersion of catalyst. On the other hand, in commercial catalysts, the XRD peaks of NiO (commercial 1 and 2) and α-Al_2O_3 (commercial 1) can be clearly identified.

Fig. 3 depicts the Ni 2p and Fe 2p core level spectra of the four pristine synthesized catalysts. Ni 2p spectra of 0Fe-0.4Ni, 0.1Fe-0.4Ni, 0.2Fe-0.4Ni and 0.5Fe-0Ni contain shake-up satellite peaks with binding energy (BE) of approx. 862 eV and peaks with BE of approx. 856 eV. In Ni-based catalysts, the binding energy of Ni^{2+} typically increases with the strength of NiO–Al_2O_3 interactions from approx. 854 eV for unsupported and weakly bound to the support NiO to approx. 856 eV for strongly bound to the support NiO [46–49]. At high NiO–Al_2O_3 interaction levels, the binding energy of Ni^{2+} in NiO of alumina supported catalysts becomes similar to that in $NiAl_2O_4$ spinel (855.8 eV) [48,50]. Due to the shift in binding energy, it is uncertain whether the Ni^{2+} state in the catalysts NiO or $NiAl_2O_4$ solely based on

Table 1
Characteristics of pristine catalysts.

| Catalysts	Bulk density (g mL^{-1})	BET surface area (m^2 g^{-1})	Total pore volume[a] (mL g^{-1})	Fe[b] (mol 100 g^{-1})	Ni[b] (mol 100 g^{-1})	Fe[b] (wt%)	Ni[b] (wt%)	Fe[b] (mol 0.5 mL^{-1}) ×10^{-3}	Ni[b] (mol 0.5 mL^{-1}) ×10^{-3}
0Fe-0.4Ni	0.99	213	0.31	0	0.389	0	22.8	0	1.90
0.1Fe-0.4Ni	0.80	187	0.21	0.100	0.422	5.6	24.8	0.4	1.69
0.2Fe-0.4Ni	0.87	150	0.17	0.193	0.384	10.8	22.5	0.84	1.51
0.5Fe-0Ni	0.85	160	0.20	0.527	0	29.5	0	2.43	0
Commercial 1	1.44	24	0.02	0	0.266	0	15.6	0	1.92
Commercial 2	1.27	90	0.10	0	0.293	0	17.2	0	1.86

[a] Based on nitrogen adsorption isotherms.
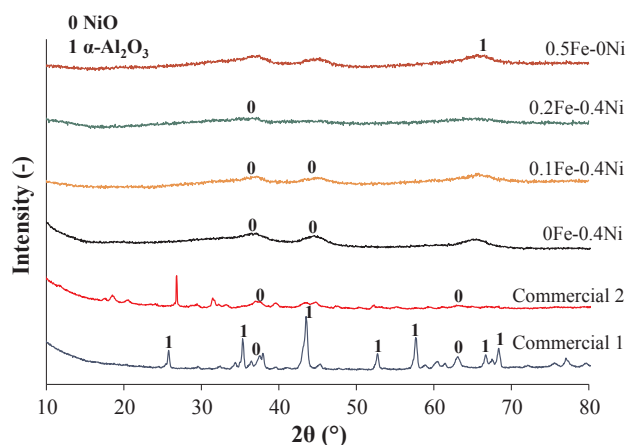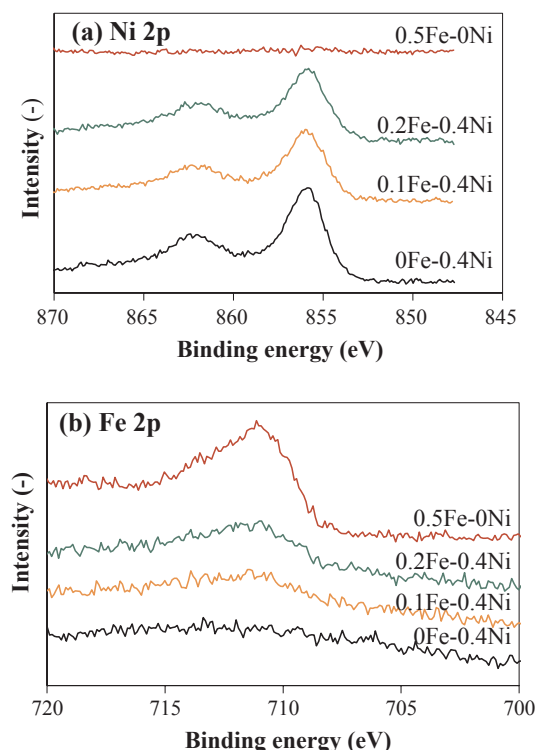
Fig. 2. XRD patterns of the pristine catalysts.

Fig. 3. Ni 2p (a) and Fe 2p (b) XPS spectra of the pristine synthesized catalysts.

XPS spectra. The similar binding energies of Ni^{2+} in all synthesized catalysts suggest that independently on Ni + Fe loading, strong interactions between NiO and alumina were maintained in the catalysts and there was no formation of new compounds with Fe species. The same can be concluded from Fe 2p core level spectra. Binding energies of Fe 2p for all catalysts were similar regardless of the presence of NiO (i.e. 711.0 eV for 0.1Fe-0.4Ni, 711.4 eV for 0.2Fe-0.4Ni and 711.0 eV for 0.5Fe-0Ni) and corresponded to Fe^{3+} in Fe_2O_3 [50].

TPR profiles provide useful information regarding reducibility of Ni and Fe oxides in the synthesized catalysts (Fig. 4). The reduction of catalysts occurred in a wide temperature range between 300 and 800 °C. The catalysts 0.2Fe-0.4Ni and 0.5Fe-0Ni contained a distinct reduction peak at 475 °C, which corresponds to the reduction of Fe_2O_3 [51], i.e. the main Fe species in catalysts according to XPS. According to the TPR profile of 0Fe-0.4Ni, most of nickel was reduced at 500–700 °C with the maximum reduction temperature at 590 °C, which can assigned to highly dispersed NiO having strong metal-support interactions [48,52]. Small shoulder peaks at 350, 425 and 770 °C were also

observed. The reduction at 300–400 °C is typically attributed to bulk and/or unsupported NiO, while the reduction > 700 °C could be attributed to nickel aluminates formed due to sintering of NiO with Al_2O_3 [48,53,54], indicating that minor quantities of these species could be also present in the synthesized catalysts. According to the similar positions of H_2 consumption peaks in the catalysts, the reducibility of Ni species was not influenced by the addition of Fe_2O_3 and vice versa.

XPS and TPR data of the commercial catalysts are shown in Fig. S2. As it was reported elsewhere [37], in both catalysts, Ni^{2+} was in the form of NiO. However, in Commercial 2, NiO was more strongly bonded to the support compared to Commercial 1. Considering the similar Ni loading per 0.5 mL catalyst bed for Commercial 1, Commercial 2 and 0Fe-0.4Ni, this allows investigation of the effects of H_2S and HCl on the activity of catalysts with different strength of $NiO–Al_2O_3$ interactions determined by the differences in porosity, crystalline structure, NiO dispersion etc. The addition of Fe to Ni-based catalyst provides further insight about the influence of H_2S and HCl on the activity of catalysts with different metal composition.

3.2. Naphthalene reforming activity

Fig. 5 depicts naphthalene conversion using the six catalysts in the presence and absence of H_2S and HCl at 850 °C. CO and CO_2 were the only reaction products. No formation of C_1–C_5 hydrocarbons was observed during the process. Naphthalene conversion over catalysts fluctuated during the first 30 min of experiment and was stabilized thereafter. In all catalysts containing Ni, the reforming activity was lower in the presence of H_2S and HCl due to the poisoning effect (data in Fig. 5a against Fig. 5b). Furthermore, naphthalene conversion by 0.5Fe-0Ni was approx. 12% in the absence of H_2S and HCl, and decreased to approx. 8% in the presence of H_2S and HCl, suggesting the poisoning of Fe. Regardless of the presence of H_2S and HCl, naphthalene conversion was stable during 5 h tests. The synthesized 0Fe-0.4Ni showed comparable conversion efficiency with commercial catalysts, which was likely due to the same amount of Ni loading per 0.5 mL bed in the three catalysts. These results suggest that there was similar poisoning effect on the naphthalene reforming activity for the catalysts with different strength of $NiO–Al_2O_3$ interactions. Reforming activity of 0.1Fe-0.4Ni was similar to 0Fe-0.4Ni, while the higher content of Fe in 0.2Fe-0.4Ni resulted in the decreased naphthalene conversion. This could be attributed to the decreased porosity and specific BET surface area with the higher Fe content due to the occupation of surface sites (Table 1). Unlike Ni-based catalysts, 0.5Fe-0Ni merely achieved approx. 8% of naphthalene conversion, indicating that Ni is more active catalyst for naphthalene reforming compared to Fe. The lower catalytic toluene reforming activity due to Fe addition to Ni/zeolite catalyst was reported by Ahmed *et al.* [38], who found the depletion in basicity strength of
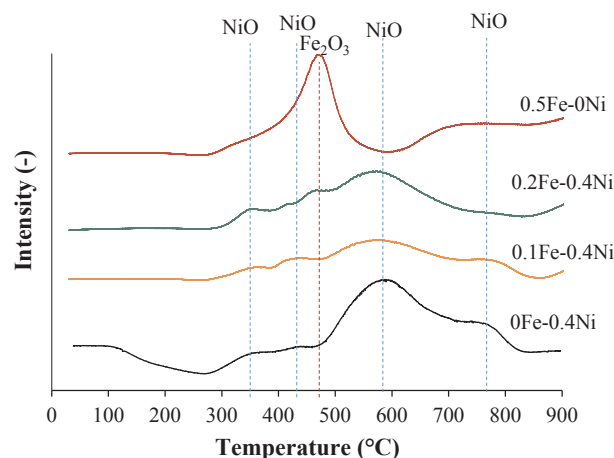

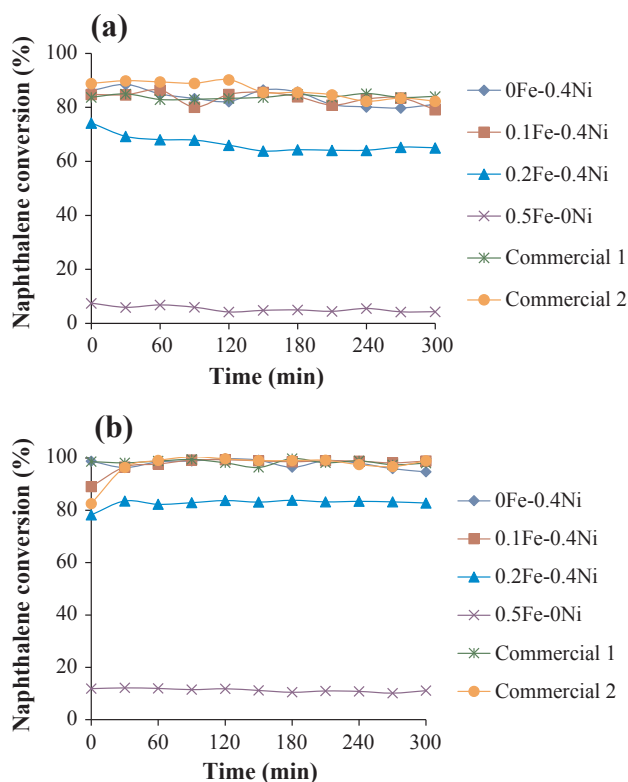**Fig. 4.** TPR profiles of the pristine synthesized catalysts.

Fig. 5. Naphthalene conversion by catalysts at 850 °C (a) in the presence of 50 ppmv H_2S and 300 ppmv HCl and (b) in the absence of H_2S and HCl.

this Fe-Ni/zeolite catalyst leading to suppressed steam reforming.

Elemental CHN analysis (Table S1) of the pristine and spent catalysts suggests that there was no significant increase in the amount of carbon after the reforming, indicating no coking happened in the presence of H_2S and HCl. This can be attributed to the relatively high content of steam in the model gas (i.e. 26 vol%) that could assist in carbon gasification.

Fig. 6 shows the TEM image of fresh 0.2Fe-0.4Ni after preheating in 20 vol% H_2–80 vol% N_2 and spent 0.2Fe-0.4Ni after 5 h of reaction at 850 °C in the presence of H_2S and HCl. The comparison of the morphologies of fresh and spent catalyst indicates the absence of carbon deposition during naphthalene reforming, which is consistent with CHN analysis. After reforming, Ni was present in the form of discreet spherical nanoparticles. This is attributed to the sintering of Ni during the process [37]. On the contrary, Fe was evenly distributed over the catalyst surface (Fig. 6a). Fig. S3 shows that in other Fe-containing catalysts, Fe also remains in the dispersed state. The coverage of entire surface of the spent 0.2Fe-0.4Ni catalyst by S and Cl indicates that the chemisorption of these species occurred both on the Ni and Fe sites (Fig. 6b) [29,55,56], which explains the poisoning effect of HCl and H_2S both on the reforming activity of Ni and Fe.

Fig. 7 shows the XRD patterns of the spent catalysts after naphthalene reforming at 850 °C in the presence of 50 ppmv H_2S and 300 ppmv HCl. In the spent samples containing Ni element, the formation of metallic Ni phase was observed as suggested by the labelled NiO XRD peaks. As there were no XRD peaks of NiO in the fresh catalysts, these results indicate that upon reduction and reforming, Ni undergoes sintering into larger size crystalline nanoparticles, which is consistent with TEM data in Fig. 6a. Unlike NiO, the formation of crystalline FeO in 0.5Fe-0Ni was not observed as suggested by the absence of corresponding XRD peaks in this sample and even distribution of Fe in the TEM images of spent catalysts (Figs. 6a and S3). According to TPR data (Fig. 4), the reforming temperature was sufficient for the reduction of Fe_2O_3 to FeO. Therefore, it is likely that in the spent

catalysts iron was in metallic non-crystalline state. These observations are consistent with scanning TEM data in Fig. 6, showing the differences in Fe morphology compared to Ni.

There was no change in the position of NiO XRD peaks in 0Fe-0.4Ni, 0.1Fe-0.4Ni and 0.2Fe-0.4Ni with the addition of Fe (Fig. 7), which would have been observed with the formation of Ni-Fe alloys [27,57], indicating that there was no alloying between Ni and Fe in the spent catalysts. The amount of chemisorbed sulfur and chlorine species during reforming was typically low which explains the absence of XRD peaks corresponding to metal chlorides and sulphides in all catalysts.

The reaction temperature is one of the most important operating variables for steam reforming. 0Fe-0.4Ni, 0.1Fe-0.4Ni and Commercial 1 were further selected to investigate the effect of temperature on catalytic activity. Fig. 8 shows naphthalene conversion at 790, 850 and 900 °C in the presence of H_2S and HCl. Except for the decrease in conversion within the initial 30 min at 790 °C, the activity of catalysts remained constant thereafter indicating that it is possible to maintain stable conversion efficiency of naphthalene in the presence of H_2S and HCl within the studied period of time at each temperature. The catalytic activities of the three catalysts were similar in the presence of H_2S and HCl at each temperature regardless of the strength of NiO–Al_2O_3 interactions (0Fe-0.4Ni vs. Commercial 1) and the addition of Fe (0Fe-0.4Ni vs. 0.1Fe-0.4Ni). The reforming activities of all catalysts were greatly influenced by the reforming temperature, increasing from approx. 40% to approx. 100% efficiencies with the increase in reaction temperature from 790 to 900 °C, respectively. These results can be attributed to the increased reaction rate of naphthalene with steam and the decreased H_2S poisoning effect at higher temperature. It has been well known that H_2S poisoning is caused by sulfur adsorbed on the nickel surface in the catalyst according to reaction (1). This reaction is reversible. With the increasing temperature desorption of H_2S increases releasing surface active sites for the steam reforming reaction [58].

To determine the respective and relative roles of H_2S and HCl in the catalyst poisoning effect observed in Figs. 5 and 8, the naphthalene reforming at four different conditions was compared: (1) 50 ppmv H_2S and 300 ppmv HCl, (2) 0 ppmv H_2S and 300 ppmv HCl, (3) 50 ppmv H_2S and 0 ppmv HCl, and (4) 0 ppmv H_2S and 0 ppmv HCl. The experiments were carried out at 790 °C, as the poisoning was the most prominent at this temperature. According to Fig. 9, in the absence of H_2S, naphthalene conversion was approx. 100% both at 0 and 300 ppmv HCl. In the presence of 50 ppmv of H_2S, naphthalene conversion decreased to approx. 40% both at 0 and 300 ppmv HCl. These results suggest that the poisoning of naphthalene reforming was caused by H_2S, while HCl had negligible effect on this reaction. Furthermore, since the naphthalene conversion in the presence of H_2S was similar at 0 and 300 ppmv HCl, it can be concluded that H_2S and HCl had no synergistic effect on the poisoning of reforming activity when both impurities were present in the stream.

Based on the obtained data, during the reforming of naphthalene from gas streams containing both H_2S and HCl, the poisoning of catalysts is mainly caused by H_2S and can be attributed to the decreased accessibility of surface active sites for hydrocarbons due to H_2S chemisorption [29]. The poisoning effect on naphthalene reforming activity was similar for the catalysts with different strength of NiO–Al_2O_3 interactions and Ni + Fe contents. Increasing reaction temperature could effectively improve catalytic activity of Ni and Ni-Fe based catalysts in the presence of H_2S and HCl leading to approx. 100% naphthalene conversion (Fig. 8).

3.3. WGS activity

Fig. 10 shows the ratios between CO and CO_2 in the gas during naphthalene reforming over the catalysts at 850 °C in the presence of H_2S and HCl. Steam reforming of hydrocarbons is typically presented as the combination of two reactions, namely, partial oxidation of hydrocarbon by steam into CO and H_2 (reaction 2) followed by WGS reaction
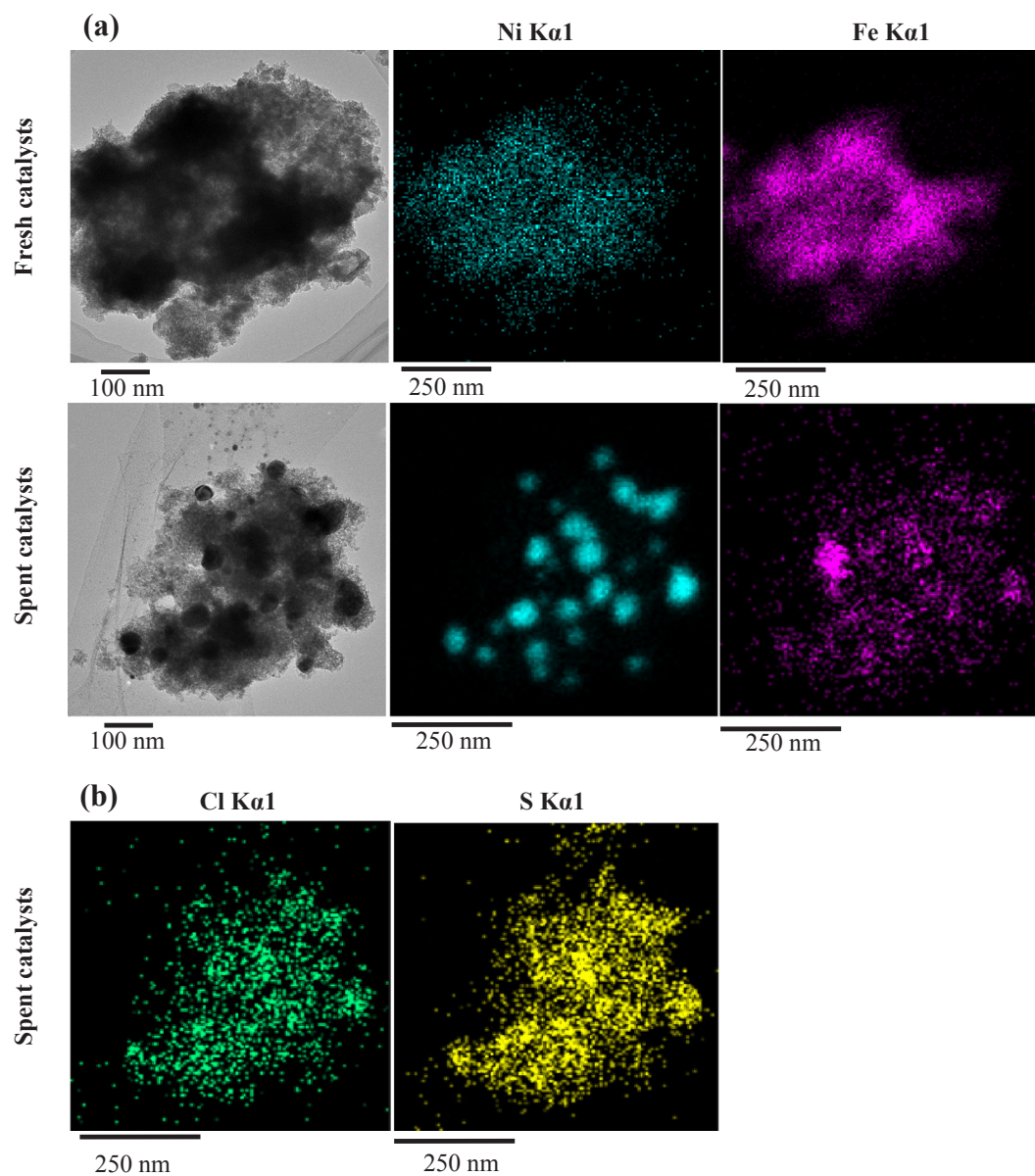
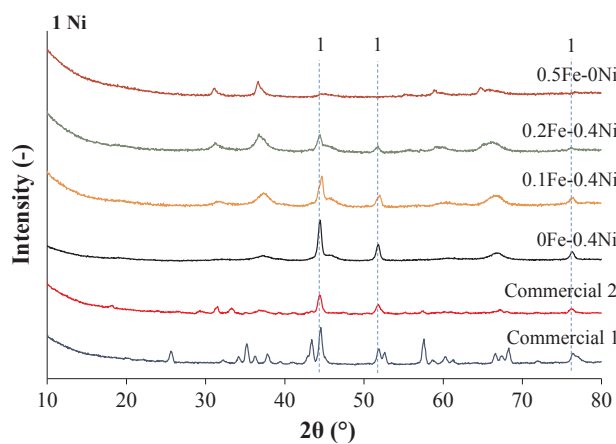**Fig. 6.** STEM mapping of fresh and spent 0.2Fe-0.4Ni: (a) Ni and Fe distribution (b) Cl and S distribution.

Fig. 7. XRD patterns of the spent catalysts after naphthalene reforming at 850 °C in the presence of 50 ppmv H_2S and 300 ppmv HCl.
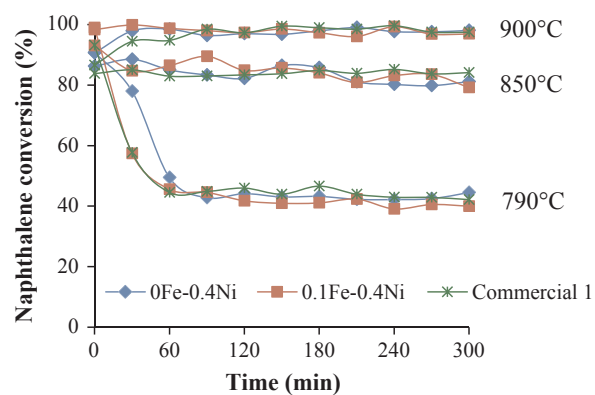

Fig. 8. Influence of temperature on naphthalene conversion in the presence of 50 ppmv H_2S and 300 ppmv HCl over 0Fe-0.4Ni, 0.1Fe-0.4Ni, and Commercial 1.
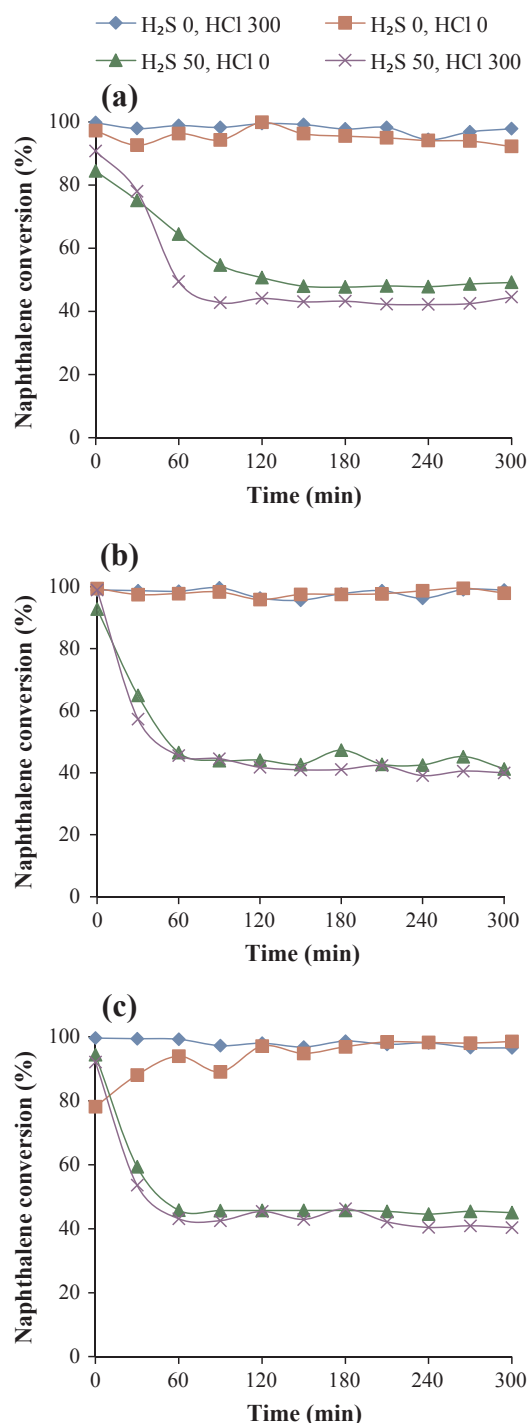
Fig. 9. Influence of H_2S and HCl on naphthalene conversion at 790 °C by (a) 0Fe-0.4Ni, (b) 0.1Fe-0.4Ni, and (c) Commercial 1.

Fig. 10. CO/CO_2 ratio of the catalysts at 850 °C (50 ppmv H_2S, 300 ppmv HCl). The dashed line represents CO/CO_2 ratio at thermodynamic equilibrium (CO/CO_2 = 0.52).

(3) [1,8,10,28,45]. Consequently, the lower CO/CO_2 ratio is probably attributed to the higher conversion of CO into CO_2 over catalysts via WGS reaction (3). Dashed black line shows the CO/CO_2 ratio at thermodynamic equilibrium (CO/CO_2 = 0.52 at 850 °C). For all catalysts, the CO/CO_2 ratios were higher than 0.52 indicating that thermodynamic equilibrium was not attainable. This is due to the lower space velocity and longer residence time required for the equilibration of WGS reaction over the catalysts [37]. There were significant differences in the kinetics of WGS reaction as suggested by the different CO/CO_2 ratios for the catalysts. The CO/CO_2 ratios of synthesized Ni and Ni-Fe catalysts increased from 0.9 to 1.0 to 1.2–1.5 during the 5 h tests,
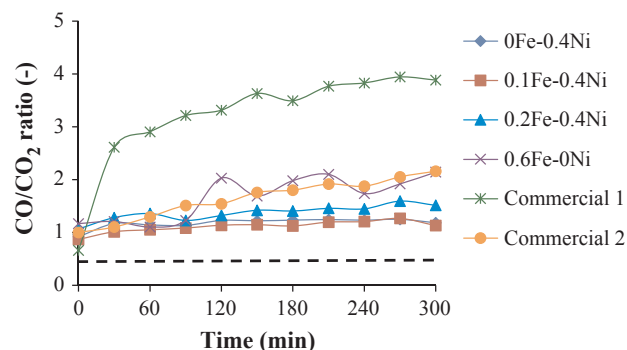
depending on the sample. These changes were much lower compared to Commercial 1 and Commercial 2 catalysts (i.e. from 0.7 to 3.9 for Commercial 1 and from 1.0 to 2.2 for Commercial 2), suggesting higher stability of WGS activity of the synthesized catalysts. Based on the similar CO/CO_2 ratios for 0Fe-0.4Ni, 0.1Fe-0.4Ni and 0.2Fe-0.4Ni, the addition of Fe to catalysts did not alter the WGS activity of catalysts. Furthermore, the lower CO/CO_2 ratios over the synthesized Ni containing catalysts compared to 0.5Fe-0Ni indicate that the WGS activity over Ni was higher compared to Fe during naphthalene steam reforming.

Although 0Fe-0.4Ni, Commercial 1 and Commercial 2 had similar NiO loading per catalyst bed volume, the strength of interactions between NiO and alumina support was different in the catalysts, eventually, leading to the different Ni-support interactions in the reduced catalysts. Specifically, the strength of interactions increased from Commercial 1 to Commercial 2 and, finally, to 0Fe-0.4Ni which is consistent with the increase in WGS activity in the same order (Fig. 10). One reason behind the observed phenomenon is the mechanism of WGS reaction over Ni based Al_2O_3 catalysts. By combining density functional theory and microkinetic modelling, it was demonstrated that Ni-support interface provides catalytically active sites for WGS reaction, serving as a storage for oxygenated Ni^{2+} species [59]. Therefore, the decrease in the strength of metal-support interactions in catalysts can result in the observed loss of WGS activity. In comparison, for the steam and dry reforming reactions of methane, the importance of metal-support interactions was found to be less important as the active sites for these reactions seem to be different. [59,60] Assuming that the mechanisms for reforming of hydrocarbons are similar [45], this could explain the negligible differences in naphthalene conversion over 0Fe-0.4Ni, Commercial 1 and Commercial 2 (as shown in Fig. 5).

For WGS reaction, oxygenated Ni^{2+} sites are required [59], while higher reforming temperatures favor the reduction of NiO to metallic Ni. TPR profiles of synthesized and commercial catalysts (Figs. 4 and S2) show that the reduction temperature of Ni^{2+} increased from Commercial 1 to Commercial 2 followed by the synthesized catalysts indicating that the synthesized catalysts can have the higher density of oxygenated Ni^{2+} sites at the reforming conditions due to the stabilization of NiO by the support [48,52,61,62]. To confirm that, thermodynamic calculations using HSC Chemistry 9 software were carried out to calculate the content of oxygenated Ni^{2+} in catalysts in the absence and presence of NiO-support interactions. For the simplicity of calculations, it was assumed that in the absence of interactions with the support, nickel can only be oxidized into NiO. In the presence of strong metal-support interactions, Ni can form stable oxidized species at the NiO-support interface. γ- and α-Al_2O_3 were selected as the representative support materials, which allow for the formation of $NiAl_2O_4$ spinel [62]. Under steam reforming conditions, H_2O acts as an oxidant and the oxidation of Ni can be described by the following
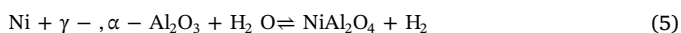
reactions:

$$Ni + H_2O \rightleftharpoons NiO + H_2 \tag{4}$$

$$Ni + \gamma-, \alpha-Al_2O_3 + H_2O \rightleftharpoons NiAl_2O_4 + H_2 \tag{5}$$

Fig. 11a shows the standard Gibbs reaction energies ($\Delta G°$) for the oxidation of Ni as the function of reforming temperature. It can be seen that $\Delta G°$ increases with temperature suggesting that higher temperature causes the formation of metallic Ni. However, at the same temperature, $\Delta G°$ is lower when γ- and α-Al_2O_3 participate in the reaction, indicating that in the catalysts with strong NiO-support interactions, there is a higher content of oxygenated Ni^{2+}. From the corresponding thermodynamic equilibrium constants, the content of Ni^{2+} can be calculated at the experimental conditions. According to Fig. 11b, in the absence of NiO-support interactions, the content of Ni^{2+} slightly increases with temperature and is 1.3%, 1.4% and 1.5% at 790, 850 and 900 °C, respectively. In the presence of NiO-support interactions, the content of Ni^{2+} is much higher at each reforming temperature (Fig. 11b). Notably, the γ-Al_2O_3 favors the stabilization of Ni^{2+} to a larger extent compared to α-Al_2O_3 highlighting the importance of alumina material for the design of catalysts with tailored WGS activity. The provided thermodynamic calculations confirm that at the reforming temperatures, NiO-Al_2O_3 interactions can indeed stabilize nickel in the oxidized form due to the participation of support in the reaction, which could be in turn responsible for the higher WGS activity on the synthesized catalysts. Since, the XRD patterns of the spent catalysts contain only metallic Ni phase (Fig. 2), it is likely that the oxygenated Ni^{2+} species are mainly present at the NiO-Al_2O_3 interface.

Previously, it was proposed that the exposure of catalysts to high concentration of HCl (2000 ppmv) during steam reforming of naphthalene causes the chemisorption of HCl on Ni followed by the sintering of Ni species into larger size nanoparticles. This process is irreversible and leads to a permanent loss of WGS activity [37]. The poisoning of WGS activity of catalysts by low concentrations of H_2S and HCl (i.e. 50 and 300 ppmv, respectively) has not been investigated. Fig. 12 presents the CO/CO_2 ratios for 0Fe-0.4Ni, 0.1 Fe-0.4Ni and Commercial 1 at 790, 850 and 900 °C. Among the tested catalysts, Commercial 1 showed the lowest WGS activity at each temperature. With the increase in temperature, CO/CO_2 ratios for Commercial 1 catalyst decreased, indicating that WGS activity of this catalyst could be improved by increasing the reforming temperature. Since the content of oxygenated Ni^{2+} species is relatively high at all reforming temperatures, this could be attributed to the faster reaction rate that allows to approach closer to the thermodynamic equilibrium and/or enhanced desorption of S- and Cl-species at higher temperature. Nevertheless, the CO/CO_2 ratios for Commercial 1 remained high compared to those corresponding to thermodynamic equilibrium. The CO/CO_2 ratios for Ni and Ni-Fe catalysts were lower than that of Commercial 1 and closer to thermodynamic equilibrium at all temperatures, indicating higher WGS activity.

Since the poisoning of Commercial 1 was more pronounced at lower temperature, the individual and combined effects of H_2S and HCl on WGS activities of two representative catalysts, namely, 0Fe-0.4Ni and Commercial 1, were compared at 790 °C. Fig. 13a presents the CO/CO_2 ratios at four experimental conditions: (1) 50 ppmv H_2S and 300 ppmv HCl, (2) 0 ppmv H_2S and 300 ppmv HCl, (3) 50 ppmv H_2S and 0 ppmv HCl, and (4) 0 ppmv H_2S and 0 ppmv HCl. In the context with respect to WGS reaction, the presence of H_2S and HCl had negligible effect on the poisoning of 0Fe-0.4Ni indicating high stability of the WGS activity to the action of both impurities. The deterioration of WGS activity of Commercial 1 was observed even in the absence of H_2S and HCl. This could be attributed to the lower strength of NiO–Al_2O_3 interactions in this catalyst compared to 0Fe-0.4Ni. As shown in Fig. 13b and c, the sizes of Ni nanoparticles were larger in the spent Commercial 1 compared to 0Fe-0.4Ni after using condition 4, which could result in the lower WGS activity [59].

For Commercial 1, CO/CO_2 ratios increased both under condition 2 (HCl only) and condition 3 (H_2S only), indicating that both impurities contributed to the poisoning of WGS activity (Fig. 13a). The poisoning of WGS activity in the presence of H_2S was faster compared to HCl as demonstrated by the rapid increase in CO/CO_2 ratio within the first 60 min of reaction (i.e. condition 2 against condition 3). The poisoning of catalyst was more pronounced in the presence of both H_2S and HCl (condition 1), indicating the detrimental synergistic effect of impurities. According to Fig. 13b and c, at low concentrations of H_2S and HCl, there was no change in the sizes of Ni nanoparticles of 0Fe-0.4Ni and Commercial 1. These data suggest that unlike at 2000 ppmv HCl in literature [37], low concentrations of H_2S and HCl are unable to enhance Ni sintering, and the detrimental effect on WGS activity of Commercial 1 was most likely associated with the poisoning of catalyst surface solely via chemisorption. This could explain the increase in WGS activity of Commercial 1 with the increase in the reaction temperature from 790 to 900 °C in Fig. 12 as higher temperature typically decreases chemisorption. If this hypothesis is correct and chemisorption is the main reason for the catalyst poisoning, after desorption of S and Cl species, the WGS activity of catalyst can be restored. On the other hand, if sintering causes the poisoning as observed for high concentrations of HCl (i.e. 2000 ppmv), the loss of WGS activity would be irreversible [37]. To test the hypothesis, the spent Commercial 1 and 0Fe-0.4Ni after 5 h of naphthalene reforming at 790 °C in the presence of 50 ppmv H_2S and 300 ppmv HCl (denoted as Exp. 1 in Fig. 14) were respectively used for the subsequent 5 h naphthalene reforming at 790 °C in the absence of H_2S and HCl (denoted as Exp. 2 in Fig. 14).
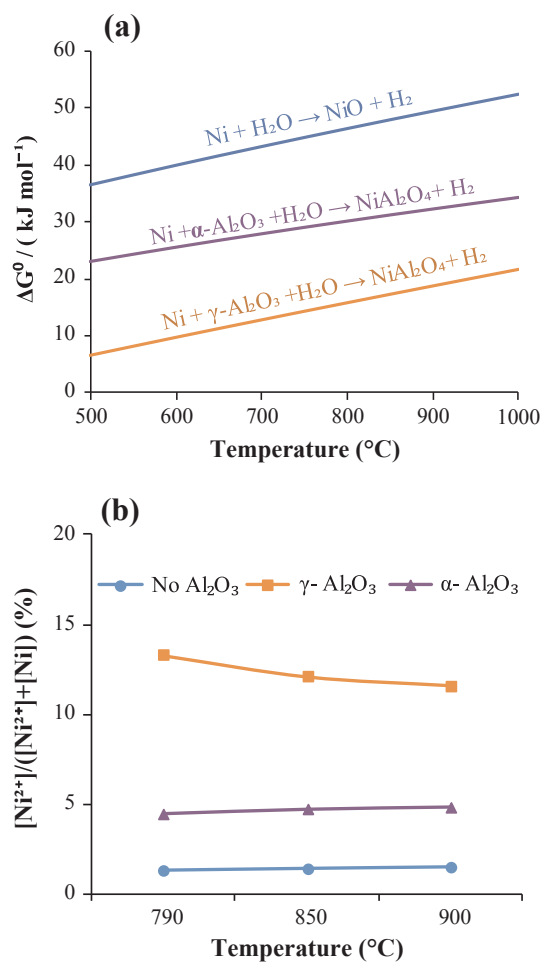

Fig. 11. (a) Standard Gibbs reaction energy for the oxidation of Ni as the function of reforming temperature and (b) the content of oxidized nickel in the presence and absence of NiO-support interactions.
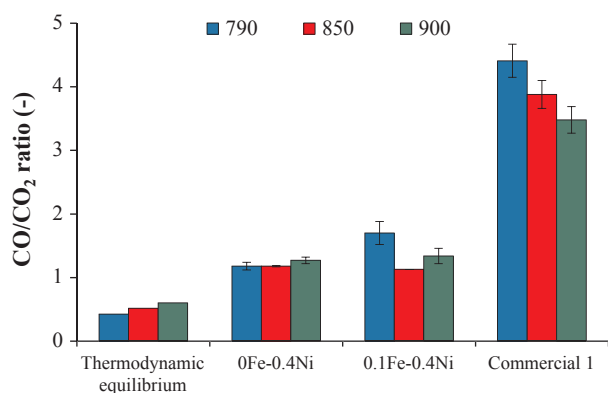
Fig. 12. Effect of temperature on CO/CO$_2$ ratio (50 ppmv H$_2$S, 300 ppmv HCl).

Fig. 13. (a) Influence of H$_2$S and HCl on CO/CO$_2$ ratio during naphthalene reforming at 790 °C. Ni particle sizes in (b) 0Fe-0.4Ni and (c) Commercial 1.
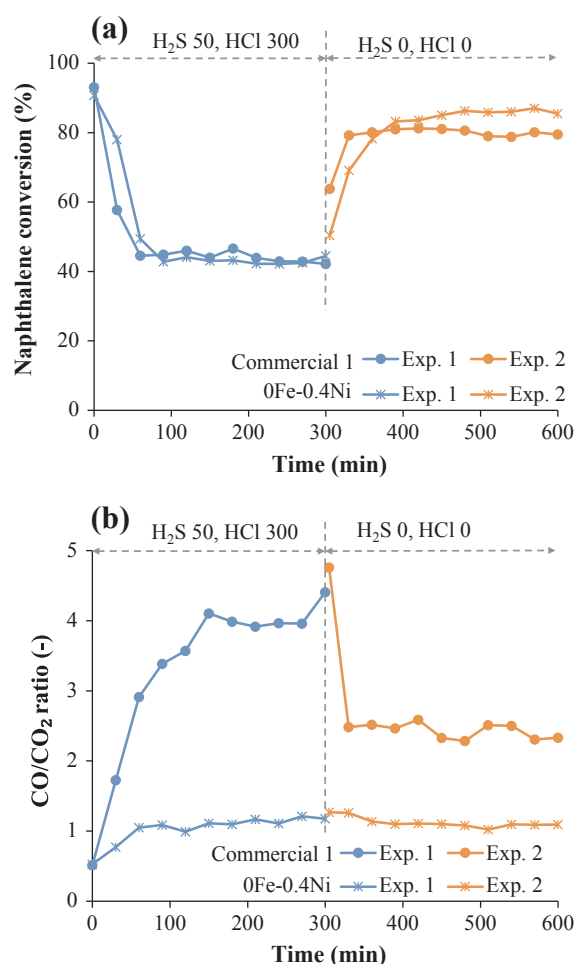

Fig. 14. (a) Naphthalene conversion and (b) CO/CO$_2$ ratio of Commercial 1 and 0Fe-0.4Ni at 790 °C: Exp.1 (fresh catalyst in the presence of 50 ppmv H$_2$S and 300 ppmv HCl) and Exp.2 (the catalyst after Exp.1 used for reforming in the absence of H$_2$S and HCl).

According to Fig. 14a, while at the end of Exp. 1 naphthalene conversions by 0Fe-0.4Ni and Commercial 1 were both only approx. 40%, they were restored to approx. 80% by commercial 1 and approx. 85% by 0Fe-0.4Ni during Exp. 2 when H$_2$S and HCl were removed from the gas stream. This improvement can be attributed mainly to the desorption of H$_2$S, that has detrimental effect on the steam reforming of hydrocarbons as it was demonstrated in Section 3.2. Despite the two times increase in the catalytic activity, naphthalene conversion during Exp. 2 was still lower compared to that of the fresh catalysts utilized in the absence of H$_2$S and HCl (i.e. approx. 100%). These data suggest that desorption of H$_2$S was incomplete. According to Fig. 14b, for 0Fe-0.1Ni, CO/CO$_2$ ratio during Exp.2 was similar with that during Exp.1 (i.e. 1.1) indicating that the presence of H$_2$S and HCl had negligible effect on WGS activity of 0Fe-0.4Ni. This observation is consistent with Fig. 13a showing high stability of the WGS activity to the action of both impurities. However, after Exp. 1, CO/CO$_2$ ratio by Commercial 1 was 4.4 and the CO/CO$_2$ ratio drastically decreased to 2.5 during the first 30 min of Exp. 2 and remained stable for 4.5 h. This value (i.e. 2.5) is comparable with the CO/CO$_2$ value obtained for the fresh Commercial 1 utilized in the absence of H$_2$S and HCl (i.e. 2.8), indicating that at low concentrations of impurities, the poisoning effect on the WGS catalytic activity was reversible, thus, confirming the hypothesis.

The structure of catalyst played an essential role in WGS reaction but not in reforming reaction (which was strongly influenced by temperature). The stronger NiO–Al$_2$O$_3$ interactions provided beneficial effect to catalytic activity which could be probably attributed to the
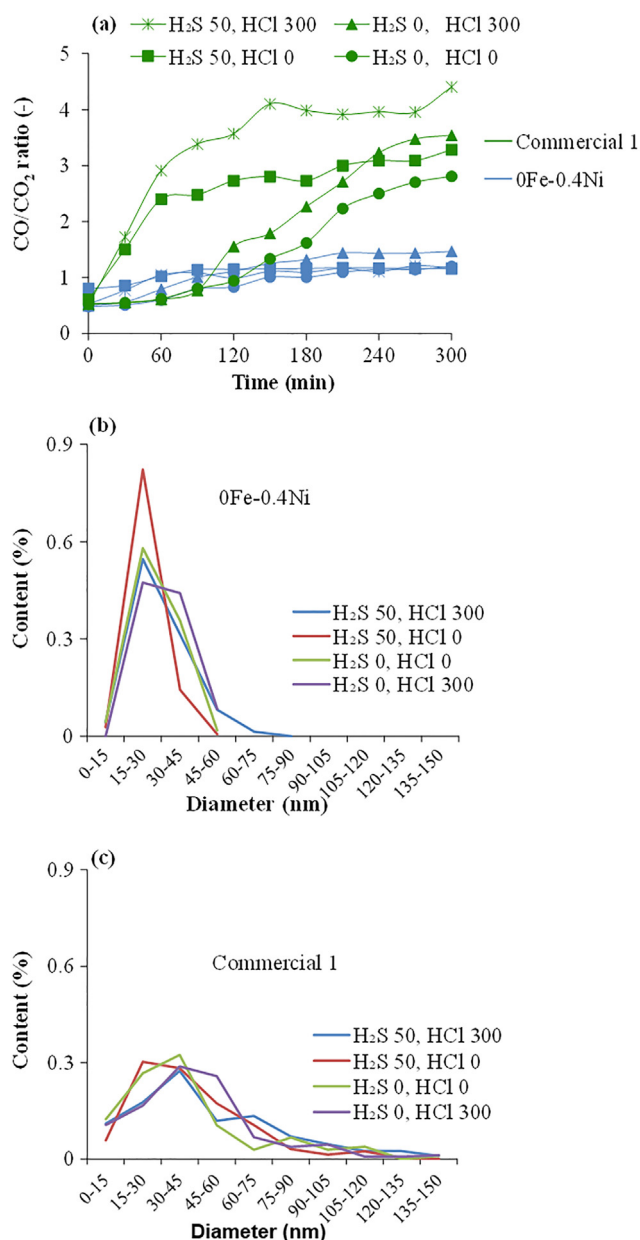
formation of larger content of oxygenated Ni^{2+} species that serve as active sites for WGS reaction [59]. The poisoning effect of HCl and H_2S on WGS was more pronounced in a catalyst with weakly bonded NiO to the Al_2O_3 support. At low H_2S and HCl concentrations, the poisoning of WGS activity proceeds via chemisorption of S and Cl species and the loss of catalytic activity is reversible when H_2S and HCl are removed from the gas stream.

4. Conclusions

The effects of H_2S (50 ppmv) and HCl (300 ppmv) on catalytic steam reforming of naphthalene were investigated using Ni, Ni-Fe and Fe catalysts supported on alumina at 790, 850 and 900 °C. Ni had higher reforming and WGS activities compared to Fe and the activities of Ni were not significantly influenced by the addition of Fe. H_2S poisoned naphthalene reforming activity of the catalysts, while the addition of 300 ppmv to gas stream had no effect on this reaction at 0 and 50 ppmv H_2S. On the contrary, both HCl and H_2S could poison WGS activity of the catalysts and the poisoning effect was more pronounced when both impurities were present in the gas stream. The poisoning by H_2S could be only partially restored by removing H_2S from the gas stream indicating the strong chemisorption of H_2S on Ni. However, H_2S poisoning effect could be prevented by carrying out reforming of naphthalene at higher temperatures. Specifically, the increase in temperature from 790 °C to 900 °C increased naphthalene conversion from approx. 40% to approx. 100%. The poisoning of WGS activity during naphthalene reforming was significantly influenced to the structure of catalyst. The stronger $NiO–Al_2O_3$ interactions provided beneficial effect minimizing the loss of WGS activity. This beneficial effect could be attributed to the formation NiO-support interfaces upon reaction serving as active sites for WGS reaction. At these concentrations of H_2S and HCl (i.e. 50 and 300 ppmv, respectively), the loss of WGS activity was reversible when H_2S and HCl were removed from the gas stream.

Acknowledgements

Appendix A. Supplementary data

Supplementary data to this article can be found online at https://doi.org/10.1016/j.fuel.2018.12.119.

References:

[1] Qian K, Kumar A. Catalytic reforming of toluene and naphthalene (model tar) by char supported nickel catalyst. Fuel 2017;187:128–36.
[2] Abu El-Rub Z, Bramer EA, Brem G. Review of catalysts for tar elimination in biomass gasification processes. Ind Eng Chem Res 2004;43(22):6911–9.
[3] Arena U. Process and technological aspects of municipal solid waste gasification. A review. Waste Manage 2012;32(4):625–39.
[4] Vehlow J. Air pollution control systems in WtE units: an overview. Waste Manage 2015;37:58–74.
[5] Sutton D, Kelleher B, Ross JRH. Review of literature on catalysts for biomass gasification. Fuel Process Technol 2001;73(3):155–73.
[6] Bain RL, Dayton DC, Carpenter DL, Czernik SR, Feik CJ, French RJ, et al. Evaluation of catalyst deactivation during catalytic steam reforming of biomass-derived syngas. Ind Eng Chem Res 2005;44(21):7945–56.
[7] Borg Ø, Hammer N, Enger BC, Myrstad R, Lindvåg OA, Eri S, et al. Effect of biomass-derived synthesis gas impurity elements on cobalt Fischer-Tropsch catalyst performance including in situ sulphur and nitrogen addition. J Catal 2011;279(1):163–73.
[8] Quitete CPB, Bittencourt RCP, Souza MMVM. Steam reforming of tar using toluene as a model compound with nickel catalysts supported on hexaaluminates. Appl Catal A 2014;478:234–40.
[9] Park HJ, Park SH, Sohn JM, Park J, Jeon J-K, Kim S-S, et al. Steam reforming of biomass gasification tar using benzene as a model compound over various Ni supported metal oxide catalysts. Bioresour. Technol. 2010;101(1, Suppl.). S101-S3.
[10] Michel R, Łamacz A, Krzton A, Djéga-Mariadassou G, Burg P, Courson C, et al. Steam reforming of α-methylnaphthalene as a model tar compound over olivine and olivine supported nickel. Fuel 2013;109:653–60.
[11] Guan G, Chen G, Kasai Y, Lim EWC, Hao X, Kaewpanha M, et al. Catalytic steam reforming of biomass tar over iron- or nickel-based catalyst supported on calcined scallop shell. Appl Catal B 2012;115–116:159–68.
[12] Liu H, Chen T, Zhang X, Li J, Chang D, Song L. Effect of additives on catalytic cracking of biomass gasification tar over a nickel-based catalyst. Chin J Catal 2010;31(4):409–14.
[13] Simell PA, Hepola JO, Krause AOI. Effects of gasification gas components on tar and ammonia decomposition over hot gas cleanup catalysts. Fuel 1997;76(12):1117–27.
[14] Dayton D. A review of the literature on catalytic biomass tar destruction. US DOE NREL Report Golden, CO 2002:510-32815.
[15] Furusawa T, Saito K, Kori Y, Miura Y, Sato M, Suzuki N. Steam reforming of naphthalene/benzene with various types of Pt- and Ni-based catalysts for hydrogen production. Fuel 2013;103:111–21.
[16] Tomishige K, Asadullah M, Kunimori K. Syngas production by biomass gasification using Rh/CeO₂/SiO₂ catalysts and fluidized bed reactor. Catal Today 2004;89(4):389–403.
[17] Iida H, Noguchi K, Numa T, Igarashi A, Okumura K. Ru/12SrO−7Al₂O₃ (S12A7) catalyst prepared by physical mixing with Ru (PPh₃)₃Cl₂ for steam reforming of toluene. Catal Commun 2015;72:101–4.
[18] Iida H, Onuki N, Numa T, Igarashi A. Steam reforming of dodecane and toluene over Ru/12SrO−7Al₂O₃ (S12A7) catalysts. Fuel Process Technol 2016;142:397–402.
[19] Ammendola P, Cammisa E, Chirone R, Lisi L, Ruoppolo G. Effect of sulphur on the performance of Rh–LaCoO₃ based catalyst for tar conversion to syngas. Appl Catal B 2012;113–114:11–8.
[20] Furusawa T, Tsutsumi A. Comparison of Co/MgO and Ni/MgO catalysts for the steam reforming of naphthalene as a model compound of tar derived from biomass gasification. Appl Catal A 2005;278(2):207–12.
[21] Li D, Ishikawa C, Koike M, Wang L, Nakagawa Y, Tomishige K. Production of renewable hydrogen by steam reforming of tar from biomass pyrolysis over supported Co catalysts. Int J Hydrogen Energy 2013;38(9):3572–81.
[22] Polychronopoulou K, Bakandritsos A, Tzitzios V, Fierro JLG, Efstathiou AM. Absorption-enhanced reforming of phenol by steam over supported Fe catalysts. J Catal 2006;241(1):132–48.
[23] Duman G, Watanabe T, Uddin MA, Yanik J. Steam gasification of safflower seed cake and catalytic tar decomposition over ceria modified iron oxide catalysts. Fuel Process Technol 2014;126:276–83.
[24] Noichi H, Uddin A, Sasaoka E. Steam reforming of naphthalene as model biomass tar over iron–aluminum and iron–zirconium oxide catalyst catalysts. Fuel Process Technol 2010;91(11):1609–16.
[25] Dong L, Wu C, Ling H, Shi J, Williams PT, Huang J. Development of Fe-promoted Ni–Al Catalysts for hydrogen production from gasification of wood sawdust. Energy Fuels 2017;31(3):2118–27.
[26] Margossian T, Larmier K, Kim SM, Krumeich F, Müller C, Copéret C. Supported bimetallic NiFe nanoparticles through colloid synthesis for improved dry reforming performance. ACS Catal 2017;7(10):6942–8.
[27] Wang L, Li D, Koike M, Koso S, Nakagawa Y, Xu Y, et al. Catalytic performance and characterization of Ni-Fe catalysts for the steam reforming of tar from biomass pyrolysis to synthesis gas. Appl Catal A 2011;392(1):248–55.
[28] Ashok J, Kawi S. Nickel-iron alloy supported over iron-alumina catalysts for steam reforming of biomass tar model compound. ACS Catal 2014;4(1):289–301.
[29] Twigg MW. Catalyst Handbook. 2nd ed. London: Manson Publishing Ltd; 1996.
[30] Yung MM, Kuhn JN. Deactivation mechanisms of ni-based tar reforming catalysts as monitored by X-ray absorption spectroscopy. Langmuir 2010;26(21):16589–94.
[31] Albertazzi S, Basile F, Brandin J, Einvall J, Fornasari G, Hulteberg C, et al. Effect of fly ash and H₂S on a Ni-based catalyst for the upgrading of a biomass-generated gas. Biomass Bioenergy 2008;32(4):345–53.
[32] Elbaba IF, Williams PT. Deactivation of nickel catalysts by sulfur and carbon for the pyrolysis-catalytic gasification/reforming of waste tires for hydrogen production. Energy Fuels 2014;28(3):2104–13.
[33] Richardson JT, Ortego JD, Coute N, Twigg MV. Chloride poisoning of water-gas shift activity in nickel catalysts during steam reforming. Catal Lett 1996;41(1):17–20.
[34] Ortego JD, Richardson JT, Twigg MV. Catalytic steam reforming of chlorocarbons: methyl chloride. Appl Catal B 1997;12(4):339–55.
[35] Coute N, Ortego JD, Richardson JT, Twigg MV. Catalytic steam reforming of chlorocarbons: trichloroethane, trichloroethylene and perchloroethylene. Appl Catal B 1998;19(3):175–87.
[36] Couté N, Richardson JT. Steam reforming of chlorocarbons: chlorinated aromatics. Appl Catal B 2000;26(3):217–26.
[37] Veksha A, Giannis A, Oh W-D, Chang VWC, Lisak G, Lim T-T. Catalytic activities and resistance to HCl poisoning of Ni-based catalysts during steam reforming of naphthalene. Appl Catal A 2018;557:25–38.
[38] Ahmed T, Xiu S, Wang L, Shahbazi A. Investigation of Ni/Fe/Mg zeolite-supported catalysts in steam reforming of tar using simulated-toluene as model compound. Fuel 2018;211:566–71.
[39] SvdH Robin Zwart, Emmen Rob, Bentzen Jens Dall, Ahrenfeldt Jesper, Stoholm Peder, Krogh Jørn. Tar Removal from Low-temperature Gasifiers. Energy research Centre of the Netherlands; 2010.
[40] Jess A. Catalytic upgrading of tarry fuel gases: a kinetic study with model

components. Chem Eng Process Process Intensif 1996;35(6):487–94.

[41] Coll R, Salvadó J, Farriol X, Montané D. Steam reforming model compounds of biomass gasification tars: conversion at different operating conditions and tendency towards coke formation. Fuel Process Technol 2001;74(1):19–31.

[42] Devi L, Ptasinski KJ, Janssen FJJG, van Paasen SVB, Bergman PCA, Kiel JHA. Catalytic decomposition of biomass tars: use of dolomite and untreated olivine. Renewable Energy 2005;30(4):565–87.

[43] Brage C, Yu Q, Chen G, Sjöström K. Tar evolution profiles obtained from gasification of biomass and coal. Biomass Bioenergy 2000;18(1):87–91.

[44] Kinoshita CM, Wang Y, Zhou J. Tar formation under different biomass gasification conditions. J Anal Appl Pyrol 1994;29(2):169–81.

[45] Musavi SZ. Design of reactor for modeling of heat transfer and kinetics in biomass tar. Reforming. 2013.

[46] Kim KS, Winograd N. X-ray photoelectron spectroscopic studies of nickel-oxygen surfaces using oxygen and argon ion-bombardment. Surf Sci 1974;43(2):625–43.

[47] Espinós JP, Gonzalez-Elipe AR, Fernández A, Munuera G. Use of XPS and Ar+ depth profiling to determine the dispersion degree of Ni in Ni/TiO₂ and Ni/SiO₂ catalysts. Surf Interface Anal 1992;19(1–12):508–12.

[48] Heracleous E, Lee AF, Wilson K, Lemonidou AA. Investigation of Ni-based alumina-supported catalysts for the oxidative dehydrogenation of ethane to ethylene: structural characterization and reactivity studies. J Catal 2005;231(1):159–71.

[49] Vedrine JC, Hollinger G, Tran Minh D. Investigations of antigorite and nickel supported catalysts by x-ray photoelectron spectroscopy. J Phys Chem 1978;82(13):1515–20.

[50] Moulder JF, Stickle WF, Sobol PE, Bomben KD. Handbook of X-ray photoelectron spectroscopy: a reference book of standard spectra for identification and inter-pretation of XPS data. Eden Prairie, MN: Physical Electronics; 1995. Google Scholar 2000:261.

[51] Kidambi PR, Cleeton JPE, Scott SA, Dennis JS, Bohn CD. Interaction of iron oxide with alumina in a composite oxygen carrier during the production of hydrogen by chemical looping. Energy Fuels 2012;26(1):603–17.

[52] Chettibi S, Benguedouar Y, Keghouche N. The metal-support interaction in the oxide supported nickel nanoparticles synthesized by radiolysis. Phys Procedia 2009;2(3):707–12.

[53] De Rogatis L, Montini T, Lorenzut B, Fornasiero P. Ni$_x$Cu$_y$/Al₂O₃ based catalysts for hydrogen production. Energy Environ Sci 2008;1(4):501–9.

[54] Norris EL. Steam reforming of methane over alumina supported nickel catalysts: influence of calcination temperature, gold doping and sulfur addition. Keele University; 2013.

[55] Xu C, Gong M, Zondlo JW, Liu X, Finklea HO. The effect of HCl in syngas on Ni–YSZ anode-supported solid oxide fuel cells. J Power Sources 2010;195(8):2149–58.

[56] Madi H, Lanzini A, Papurello D, Diethelm S, Ludwig C, Santarelli M, et al. Solid oxide fuel cell anode degradation by the effect of hydrogen chloride in stack and single cell environments. J Power Sources 2016;326:349–56.

[57] Gheisari K, Javadpour S, Oh JT, Ghaffari M. The effect of milling speed on the structural properties of mechanically alloyed Fe–45%Ni powders. J Alloy Compd 2009;472(1):416–20.

[58] Srinakruang J, Sato K, Vitidsant T, Fujimoto K. Highly efficient sulfur and coking resistance catalysts for tar gasification with steam. Fuel 2006;85(17):2419–26.

[59] Foppa L, Margossian T, Kim SM, Müller C, Copéret C, Larmier K, et al. Contrasting the role of Ni/Al₂O₃ interfaces in water-gas shift and dry reforming of methane. J Am Chem Soc 2017;139(47):17128–39.

[60] Jones G, Jakobsen JG, Shim SS, Kleis J, Andersson MP, Rossmeisl J, et al. First principles calculations and experimental insight into methane steam reforming over transition metal catalysts. J Catal 2008;259(1):147–60.

[61] Santamaria L, Lopez G, Arregi A, Amutio M, Artetxe M, Bilbao J, et al. Influence of the support on Ni catalysts performance in the in-line steam reforming of biomass fast pyrolysis derived volatiles. Appl Catal B 2018;229:105–13.

[62] Giehr A, Maier L, Schunk SA, Deutschmann O. Thermodynamic considerations on the oxidation state of Co/γ-Al₂O₃ and Ni/γ-Al₂O₃ catalysts under dry and steam reforming conditions. ChemCatChem 2018;10(4):751–7.